

# Mode Switching and Subpulse Drifting in PSR B0826–34

A. Esamdin<sup>1,2,4,5</sup>, A. G. Lyne<sup>2</sup>, F. Graham-Smith<sup>2</sup>, M. Kramer<sup>2</sup>,  
R. N. Manchester<sup>3</sup>, X. Wu<sup>1,4</sup>

<sup>1</sup>*Urumqi Observatory, National Astronomical Observatories, CAS, 40 South Beijing Road, Urumqi 830011, China*

<sup>2</sup>*Jodrell Bank Observatory, Manchester University, UK*

<sup>3</sup>*Australia Telescope National Facility, CSIRO, P.O. Box 76, Epping NSW 1710, Australia*

<sup>4</sup>*Department of Astronomy, Peking University, Beijing 100871, China*

<sup>5</sup>*Chinese Academy of Sciences - Peking University Beijing Joint Astrophysics Center, Beijing 100871, China*

Accepted 0000 December 00. Received 2004 December 14; in original form 2004 October 11

## ABSTRACT

We present high-quality observations of PSR B0826–34 at 1374 MHz. The emission from this pulsar exhibits strong bursts of pulses followed by long periods of ‘null’ pulses. When it is strong, the radiation extends through the whole pulse period. We show for the first time that there is weak emission during the ‘null’ phases, which should therefore be considered to be a different mode rather than a null. During this weak mode the profile is similar to that observed in the strong mode at low radio frequency. Using a phase-tracking method, the pattern of drifting subpulses during the strong mode is seen to be coherent across the whole profile. The drift rate is variable and includes positive and negative values. Thirteen subpulse bands have been directly observed, covering the whole longitude range. The subpulses and their spacings ( $P_2$ ) are wider in one half of the profile than those in the other half. This difference, and the variation of observed  $P_2$  within the two regions, can be accounted for if the magnetic pole is inclined to the rotation axis by about  $0.5^\circ$ . These two regions appear to represent radiation from outer and inner cones. The intensity modulation of subpulses in all longitude ranges is related to the magnitude of the drift rate.

**Key words:** radiation mechanisms: non - thermal - pulsars: general - pulsars: individual: B0826–34

## 1 INTRODUCTION

PSR B0826–34 (PSR J0828–3417) is known as a pulsar whose emission extends through the whole pulse period ( $P = 1.848$  sec). It is a relatively old pulsar with a characteristic age of  $3 \times 10^7$  yr. PSR B0826–34 exhibits some extreme forms of subpulse drifting behaviour, and it switches between strong and weak emission modes. The weak mode is so weak that it has long been regarded as a complete null (Biggs et al. 1985, B85 hereafter).

PSR B0826–34 was discovered during the second Molonglo pulsar survey (Manchester et al. 1978). An early study of this pulsar by Durdin et al. (1979) at 408 MHz showed that the pulsar appears to exhibit pulse nulling for at least 70 per cent of the time with observed null intervals from a few to 15 000 periods. The drifting subpulses in this pulsar were first observed by B85. The integrated pulse profile and most individual pulses extend over all longitudes of the pulse period, implying that this pulsar is an almost aligned rotator (i.e. the inclination angle between the rotation and magnetic axes is very small), and that it is viewed from a

direction close to the rotation axis. At 645 MHz, B85 found 5 to 6 bands of drifting subpulses in part of the profile, and noted that the drift rate of these bands shows wide variation, including sign reversals but with no significant variations in the drift-band spacing ( $P_2$ ).

We have recorded two long sequences of individual pulses from PSR B0826–34 at 1374 MHz. At this frequency, there is strong emission through most of the pulse period which allows us to investigate the pattern of drifting subpulses in the strong mode and to trace this pattern round a complete track in the emitting region.

## 2 OBSERVATIONS AND DATA

The single-pulse observations used in our analysis were made with the 64-m Parkes radio telescope using the central beam of the multibeam receiver system at 1374 MHz (Manchester et al. 2001). The receiver system recorded two orthogonal polarizations in 96 channels, each with 3-MHz bandwidth. The channel outputs were delayed to compensate for the

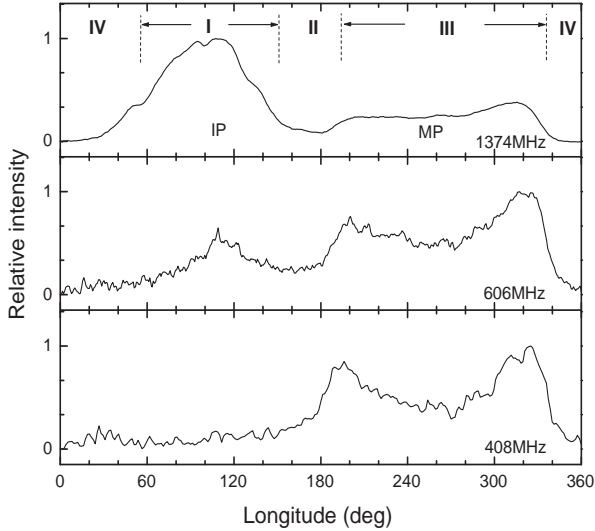


**Figure 1.** Integrated profiles for the strong mode of PSR B0826–34 at 1374, 606 and 408 MHz, showing the profile evolution with frequency. The whole longitude is divided into four regions (I, II, III, IV) according to the difference in emission and subpulse drifting properties.

effect of interstellar dispersion, using a dispersion measure of  $65.6 \text{ cm}^{-3}\text{pc}$ , and then summed.

Two long-duration single-pulse sequences were obtained on 2002 Sept 10 and Nov 1. The first sequence (A), lasting 6 hours, was sampled at 2 millisecond intervals; the second (B), lasting 3.9 hours, was sampled at 0.5 millisecond intervals.

Sequences of several thousand strong pulses, which we note as strong emission blocks, are typical for this pulsar. Data set A comprised 11670 individual pulses, with about 5900 continuously in a strong emission block. Data set B comprised 7530 individual pulses, 3900 of which were continuously in a strong emission block. These statistics are similar to those reported by B85.

### 3 INTEGRATED PULSE PROFILES

Fig. 1 shows integrated pulse profiles obtained in the strong mode at three radio frequencies. The average profile at 1374 MHz was obtained by integrating all individual pulses within the strong emission block of data set A. The point of minimum intensity through the profile was defined as both the zero of longitude and the zero of intensity. The profile at 606 MHz was recorded in 1998 using the Lovell telescope, and the profile at 408 MHz is taken from B85. The profiles at two lower frequencies were aligned with the profile at 1374 MHz by the centroid of the main pulse as described below.

We divide the profile into four regions as shown in Fig. 1. Regions I and III, covering longitudes  $56^\circ < l < 150^\circ$  and  $195^\circ < l < 338^\circ$  respectively, display the most obvious drifting subpulses at 1374 MHz; regions II and IV are two bridge regions with weaker subpulses. The components designated as main-pulse (MP) and inter-pulse (IP) by B85 are within region III and region I respectively. Region I is very

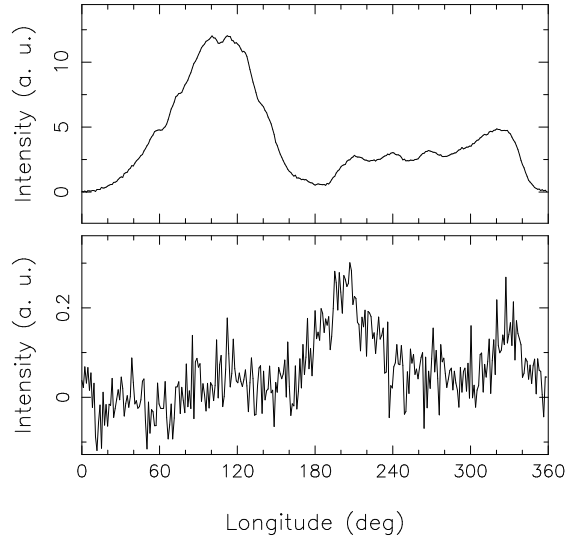


**Figure 2.** Integrated profiles for the strong (upper panel) and weak emission mode (lower panel) of PSR B0826–34 at 1374 MHz. Each profile was obtained from averaging 2048 individual pulses. The units of intensity are arbitrary, but the same in the two plots and in Figs. 3, 8 and 9; the lower plot is expanded by a factor of about 45.

weak at 408 MHz, but it contains about 24% and 67% of the profile energy at 606 and 1374 MHz respectively.

#### 3.1 The weak mode

The weak mode that follows the ‘normal’ or strong mode shown in Fig. 1 generally lasts longer than the strong emission sequences. We have integrated all pulses received in these apparent ‘nulls’ and find that the pulsar is in fact detectable at 1374 MHz during this time. Fig. 2 shows the profiles obtained in the strong and weak modes. The weak mode profile is found to be similar to this in intensity and shape for shorter integrations of 1000 periods throughout our observations.

Not only is the mean intensity of the weak mode only about 2% of that of the strong mode, but there is also a marked difference between the two profiles. The pulse profile of the weak mode extends through at least half of the period, showing a double peak covering region III; the profile is similar to that of the strong mode at lower frequencies (Fig. 1). No significant transient effects in pulse phase or intensity were observed at the transitions between the two modes.

### 4 SUBPULSE DRIFTING

Fig. 3 presents two sequences of single pulses from both data sets in the form of a longitude-time diagram. Each contains 1000 successive pulses in a strong emission sequence. The drifting pattern of subpulses noted by B85 is seen to extend through the whole pulse period, although it is indistinct in regions II and IV.

In this paper, we define the drift rate ( $D$ ) of the drifting

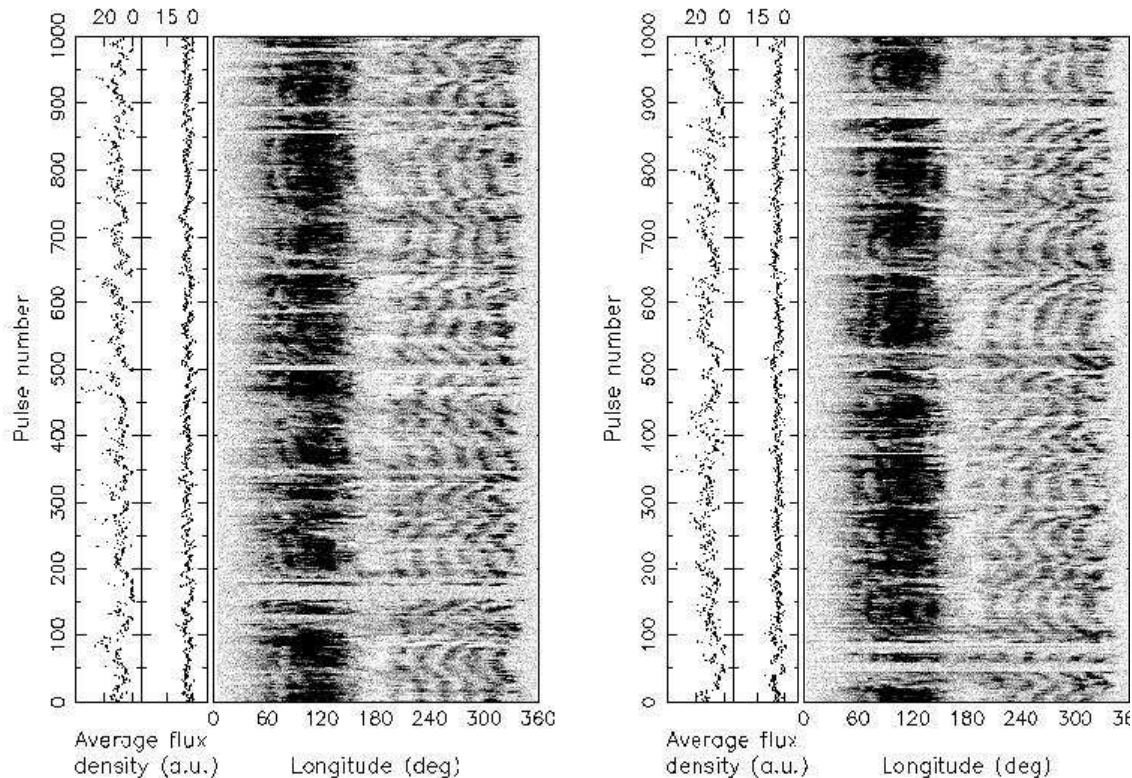


**Figure 3.** Two sequences of 1000 individual pulses in strong emission mode sequences within data sets A (left) and B (right) presented in grey scale, showing the pattern of subpulse drifting extending through the whole period. The two panels on the left side of each grey scale diagram (i.e. longitude-time diagram) show the variation in average flux densities in regions I (left) and III (right) as a function of pulse number. The units of flux density are arbitrary, but the same in all plots and as in Figs. 2, 8 and 9.

subpulses as  $D = \Delta l$  per period ( $^{\circ}/P$ ), where  $\Delta l$  is the absolute longitude shift in degrees during one pulse period  $P$ . A negative value indicates a drift from late to earlier longitudes, while a positive one indicates a drift from early to later longitudes.

#### 4.1 Phase tracking and drifting subpulse integration

Due to the weakness of the subpulses in region II and IV, we investigate the drift behaviour in these regions most easily in relation to the subpulse structure in region III, where the subpulse phase can be determined unambiguously. The positions of subpulses in regions I, II and IV are then studied relative to those in region III.

The drift phase of the whole pattern was found by extracting the phases of subpulses within region III by convolution with an appropriate template in a similar manner to that used by Lyne & Ashworth (1983) in studying PSR B0809+74. This template was obtained in the first instance by choosing a part of the profile within longitude range from  $220^{\circ} - 300^{\circ}$ . The subpulse phase in each separate profile of the whole series was then found by determining the position of the peak of the convolution of the template with

the data in this longitude range. Across this region the separation of the subpulses is essentially constant and there is little amplitude variation from subpulse to subpulse, so that the subpulse phase is well-determined by this method. An improved template was then obtained by adding together a few dozen strong pulses which all had the same phase as the original template and extracting the appropriate portion of the resulting profile (Fig. 4).

The individual pulses were then divided into ten groups, corresponding to equal intervals of subpulse phase. All pulses in each of the ten phase intervals were then co-added, producing the ten profiles shown in the central panel of Fig. 5. A coherent pattern of subpulses can be seen across much of the period, showing that the subpulse phenomenon is essentially coherent through the whole profile.

Each of these ten integrated profiles shows the drifting subpulses on top of a substantial non-drifting contribution to the profile. In order to improve the visibility of the subpulses, the integrated profile (top panel in Fig. 5), produced from all single pulses in the strong mode, was then subtracted from each profile to give the ten profiles shown in the bottom panel in Fig. 5. These ten profiles show the integrated subpulse pattern in ten phases of the drift. The ten profiles are presented in grey-scale format in Fig. 6, re-

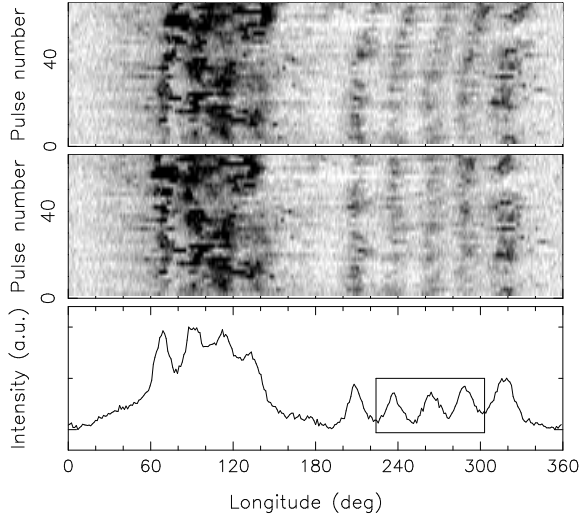


**Figure 4.** Construction of a template to follow the drifting phases of subpulses. The chosen section of profile in longitude range  $220^\circ - 300^\circ$  includes three distinct drifting subpulses. The drift phase of each of a series of 66 successive pulses (shown in the upper panel) was found by convolution with an initial template obtained from a single strong pulse. The pulses are again shown in the central panel, after adjusting their relative phases, and their sum is shown in the lower panel (the units of intensity are arbitrary). This template, in the same longitude range, was used to find the drift phase of all single pulses in the strong emission mode in both data sets.

peating twice in longitude and 14 times in phase, allowing the weak subpulses in regions II and IV to be followed by eye. The successful integration of all subpulses to produce Fig. 6 shows that the pattern is stable and repeatable over the whole data set.

#### 4.2 The pattern of subpulse drifting

The drifting subpulses which can be seen through the whole range of longitude comprise 13 successive drifting sub-bands, labelled A to M in Fig. 6. The drifting subpulse pattern continues through the longitude region around the minimum of intensity in the integrated profile, confirming that there are regularly drifting subpulses in the whole longitude range. The least distinct pattern throughout the diagram appears in the longitude range  $20^\circ < l < 56^\circ$ . (Note, however, that there is significant integrated-profile energy in this range and at all longitudes, as shown in the top panel in Fig. 6; this may not be directly related to the drifting subpulses.)

#### 4.3 The spacing ( $P_2$ ) and width (FWHM) of drifting subpulses

As can be seen in Fig. 3, and more clearly in Fig. 6, the longitude intervals between subpulses ( $P_2$ ) are different in the two prominent regions I and III, and they vary slightly with longitude.  $P_2$  ranges from  $19^\circ$  to  $23.5^\circ$  in region I and from  $26.8^\circ$  to  $28^\circ$  in region III; in our later discussion we use average values of  $22.2^\circ$  and  $27.5^\circ$  for these regions. (B85 reported that the average  $P_2$  in region III at 645 MHz is  $29^\circ$ ).

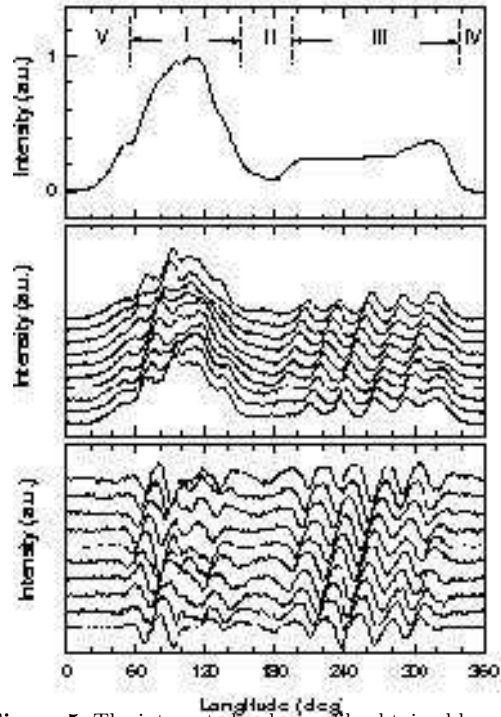


**Figure 5.** The integrated pulse profile obtained by adding a total of 9800 individual pulses from the two strong emission sequences (upper panel), and the integrated profiles obtained by selecting pulses in ten separate contiguous subpulse phase bins (central panel). The lower panel of ten profiles was obtained by subtracting the integrated pulse profile from the ten separate profiles. The units of intensity are arbitrary and different in the three diagrams.

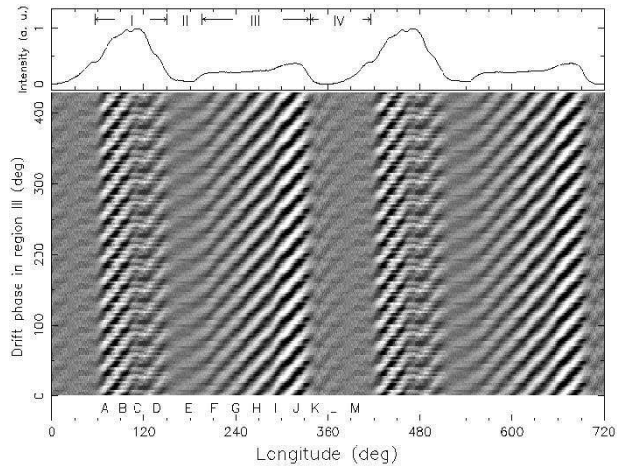


**Figure 6.** Integrated drifting subpulse diagram in grey scale (lower panel). In this presentation the pattern of the ten remnant profiles in the lower panel of Fig. 5 is repeated twice in longitude and 14 times in subpulse phase, allowing the weak subpulses in regions II and IV to be followed by eye. 13 drifting subpulses across one pulse period are labelled A to M. The differences in inclination of the dark stripes indicates the variation of subpulse spacing in different longitude regions. The integrated pulse profile (repeated twice in longitude) is shown in the upper panel with arbitrary intensity scale.

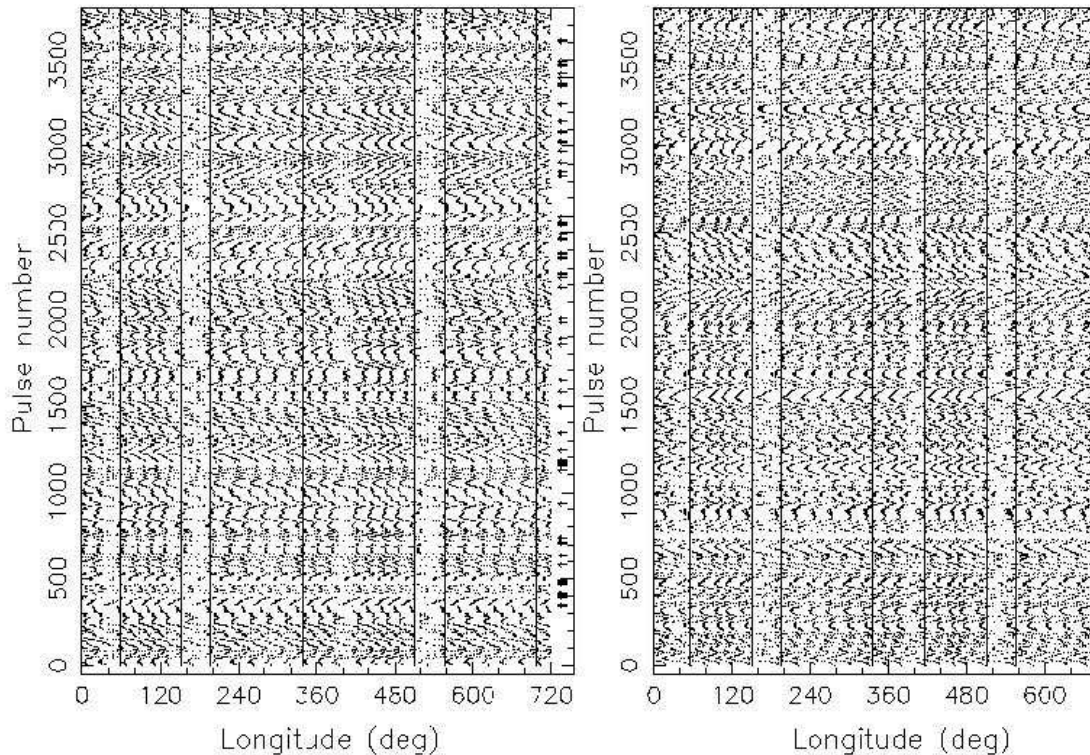


**Figure 7.** Drifting patterns from data set A (left panel) and data set B, each produced by 3800 single pulses, showing the large time scale drifting property of the pulsar. The positions of drifting subpulses are presented as dots. The pattern extends twice in longitude to show more clearly the drifting in region IV. The vertical lines in the diagrams indicate the four defined longitude regions. The drifting pattern was interrupted by pulses in weak emission mode, lasting for 1 to 40 periods, indicated by arrows on the right side in both panels.

The full width at half maximum (FWHM) of drifting subpulses in regions I and III was measured using 20 short sequences of single pulses from both data sets. Each sequence contained 20 successive single pulses in a nearly stationary state (i.e. drift rate  $D < 0.5^\circ$  in either drift direction). For each sequence, the single pulses were co-added after adjusting phases of drift to produce one profile. The subpulses in region I appear to overlap; we therefore fitted Gaussian curves to obtain the FWHM for each component.

The FWHM of drifting subpulses in region III ranges from  $10.7^\circ$  to  $14.7^\circ$ , with an average of  $13.1^\circ \pm 1.9^\circ$ . Strong subpulses tend to be wider, and to occur in the later longitudes of the region.

The FWHM of subpulses in region I ranges from  $16^\circ$  to  $24^\circ$ , with an average of  $19^\circ \pm 3.5^\circ$ . Strong subpulses again tend to be wider; they tend to occur around the middle of the region.

#### 4.4 The variable drift rate of the whole pattern

Using the drift phase of each pulse, determined as in Section 4.1, we plotted the position of each subpulse in all 7600 single pulses of both data sets as shown in Fig. 7. The short sequences of weak-mode pulses, within which the drift phase could not be traced, are indicated by arrows.

The subpulse pattern can drift from early to later longi-

tudes (positive drift) or from late to earlier longitudes (negative drift). The transition from negative to positive drift is usually smooth, while the transition from positive to negative drift is often abrupt. The most rapid drifting, both positive and negative, occurs immediately before and after these abrupt transitions, which we refer to as turning points. At least four abrupt transitions of drift directions from positive to negative were also noticed by B85, designated by them as a ‘runaway’ effect, in a sequence of about 2860 single pulses at 645 MHz. Our data sets suggest that the progress from turning point to turning point is a repeating pattern, with a time scale ranging from tens to some hundreds of pulsar periods.

The drift rate in region III ranges from about  $-3.2^\circ/P$  (late to early) to about  $3.6^\circ/P$  (early to late), changing continuously within some tens to several hundreds of pulse periods. This range is significantly larger than that from  $-1.5^\circ/P$  to  $2.1^\circ/P$  measured by B85 at 645 MHz; their smaller value for the range may however be due to the lower signal-to-noise ratio of their data.

As shown in Fig. 3 and Fig. 7, the average drift rate of drifting subpulses in region I is slightly smaller than that in region III. In region II, as well as in longitude range  $20^\circ < l < 56^\circ$ , the drifting subpulses present a larger drift rate than others within the whole longitude range.

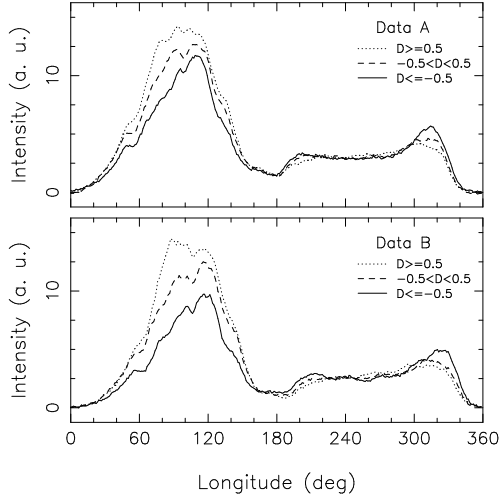


**Figure 8.** Integrated profiles produced by single pulses in three drift rate ( $D$ ) ranges measured in region III,  $D \geq 0.5^\circ/P$  (solid line),  $|D| \leq 0.5^\circ/P$  (dashed line) and  $D \leq -0.5^\circ/P$  (dotted line). The upper and lower panels show the profiles obtained from data sets A and B respectively. The units of intensity are arbitrary, but the same in both panels and as in Figs. 2, 3 and 9.

## 5 INTENSITY MODULATION

B85 noted that strong subpulses in region I occurred more frequently when the drift was from early to later longitudes. We looked for and found similar effects in our observations. In Fig. 8, we compare the integrated profiles produced by single pulses within three drift rate ranges so as to show the variation of average profile intensity in three different drift states. The drift ranges we chose to produce these average profile are  $D \geq 0.5^\circ/P$ ,  $D \leq -0.5^\circ/P$  and  $|D| < 0.5^\circ/P$ , measured in region III. Relative to the average profiles produced by pulses with the most negative drift rates (solid lines), the profiles corresponding to the small (dashed) and most positive (dotted) drift rates have increasingly enhanced intensity in the whole of region I, while the profile around the leading and trailing edges of region III is weakened. These differences are important in our discussion of the possible role of aliasing in our interpretation of the drifting subpulse pattern.

The dependence of pulse profile on drift rate can also be followed for individual pulses by integrating the intensity separately over regions I and III, as shown in Fig. 9. Here the two plots (repeated for the two data sets A and B) show the intensities of single pulses averaged in regions I and III as a function of drift rate. The average intensities used in these plots are shown on the left and right hand sides respectively of the longitude-time diagrams in Fig. 3. The modulation of average flux density in these regions is clearly associated with the drift rate. The two top panels in Fig. 9 (from the two data sets) confirm the conclusion from Fig. 8 that the emission in region I increases with the increasing drift rate, while the two lower panels show a small opposite effect in region III.

As we noted in the previous section, the drift behaviour of the pulsar frequently follows a repeating pattern from turning point to turning point. Generally, the whole pattern of subpulses drifts from late to earlier longitudes, is

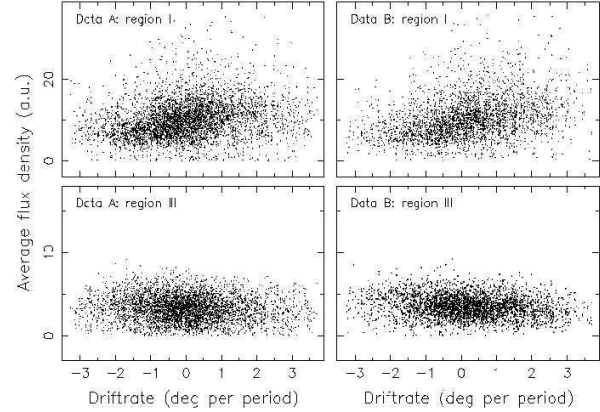


**Figure 9.** Average flux densities in region I and III of single pulses as a function of drift rate. The upper-right and lower-right panels show the average flux densities in region I and III from data A respectively. The upper-left and lower-left panels show the average flux densities in region I and III from data B respectively. The units of flux density are arbitrary, but the same in all panels and as in Figs. 2, 3 and 8.

stable for several pulses, and then drifts from earlier to later longitudes. Fig. 9 implies that the intensity modulation of the pulsar follows the same cycle as the drift. Frequently, subpulse emission in region III rises significantly in pulses immediately before the turning points, and it drops significantly at the beginning of the next drifting cycle.

Previous studies in a number of other drifting pulsars have noticed that the changing of integrated profile shape is associated with a variation of drift rate. This has been observed in B0031-07 (Huguenin et al. 1970), B0809+74 (Lyne & Ashworth 1983; Davies et al. 1984; Van Leeuwen et al. 2002), B1112+50 (Wright, Sieber & Wolszczan 1986), B1918+19 (Hankin & Wolszczan 1987), B1944+17 (Deich et al. 1986), B2319+60 (Wright & Fowler 1981), although no reversal of drift direction is involved in these pulsars.

The variability of observed drift rate of the pulsar, including reversals of the drift direction, appears to be inconsistent with the  $\mathbf{E} \times \mathbf{B}$  drift of sparks described by Ruderman & Sutherland model (Ruderman & Sutherland 1975). Gupta et al. (2004) note, however, the possibility that the observed drift rate is aliased by the rotation rate of the pulsar, in which case the drift could be in a constant direction with small variations in rate. This would require a remarkable coincidence between the drift rate and the average subpulse spacing, so that the drift pattern moves by one subpulse interval in one rotation. Our observations make this interpretation unlikely; the existence of cusps in the drift pattern, and the difference between the intensity profiles for positive and negative drift suggest strongly that the simpler explanation is correct, so that the drift is indeed reversing its direction of motion.

## 6 THE GEOMETRY OF THE POLAR CAP

It has already been pointed out that the wide pulse profile indicates that this pulsar is observed nearly pole-on, with a small inclination angle between the magnetic and rota-

tion poles. The line of sight follows a circular path round the rotation pole. We now suggest that this circular path is within and close to the edge of a polar cap of emission whose centre is displaced from the rotation pole by a small angle, as shown in Fig 10. The 13 subpulses then correspond to a set of 13 emitters spaced uniformly in angle around the magnetic pole. The whole pattern drifts around the pole in either direction at a rate of up to  $3^\circ$  to  $4^\circ$  per rotation period (1.8 sec).

The drift pattern is clearly defined in regions I and III, but in regions II and IV the drift is more confused. There is a difference in subpulse spacing  $P_2$  between regions I and III, in which the average values of  $P_2$  are  $22.2^\circ$  and  $27.5^\circ$  respectively. We interpret this in terms of the offset of the circular path of the line of sight from the centre of the polar cap, as shown in Fig. 10. The difference in subpulse spacing is then accounted for as a difference in radial distance between the line of sight and the magnetic pole. The emitting regions extend radially, so that the line of sight cuts the array of emitters in a circle, radius  $\rho$ , centred on the rotation pole R. The magnetic pole M is at a small angular distance  $\alpha$  from R, so that the angle between the line of sight and M varies between  $\rho + \alpha$  and  $\rho - \alpha$ . The observed ratio of subpulse spacing is 1.22, giving

$$\frac{\rho + \alpha}{\rho - \alpha} = 1.22 \quad \text{and hence} \quad \alpha = 0.1\rho. \quad (1)$$

The geometry can be determined in principle from measurements of the linear polarisation, but the position angle swing is complex (Lyne & Manchester 1988), and possibly confused by orthogonal polarisation mode switching. Single pulse polarisation observations are required to reconstruct the underlying mode-corrected position angle swing (Gil & Lyne 1995). The typical value for the diameter of the polar cap is  $\sim 13^\circ P^{-1/3}$  (Lyne and Manchester 1988), i.e.  $10^\circ$  for B0826-34. If we assume that the line of sight is close to the edge of the polar cap, so that the radius  $\rho \approx 5^\circ$ , we find that the inclination angle  $\alpha = 0.5^\circ$ .

The weakness of the subpulses in regions II and IV, and the poor definition of their tracks in Fig. 6 suggests that there may be a radial variation of emitter strength. This would accord with the suggested identification of inner and outer cone components in the integrated pulse profiles of many pulsars observed at large polar angles  $\alpha$  (Rankin 1983, 1993a, 1993b; Gil, Kijak & Seiadakis 1993; Kramer et al. 1994). Such an explanation requires that the conal structure for an almost perfectly aligned pulsar such as B0826–34 is similar to that of much more oblique rotators. On the other hand, it is possible that regions I and III are simply areas of enhanced emissions from bright regions over a randomly patchy polar region as suggested by Lyne & Manchester (1988).

We regard the moding behaviour as a change in a pattern of excitation underlying the whole of the polar cap; it is not yet possible to say whether the subpulse drifting continues in the weak mode.

## 7 SUMMARY

The main results of this work are as follows:

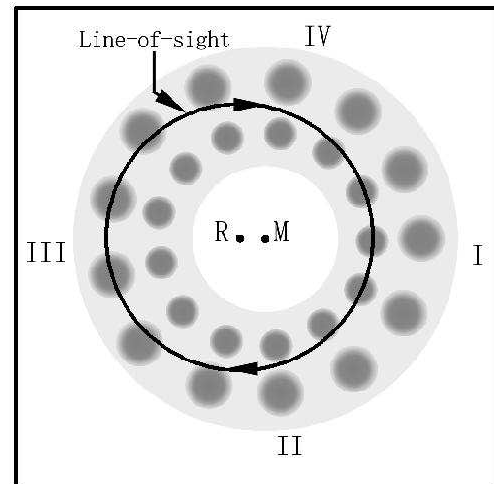


**Figure 10.** Map of the polar cap. The subpulse emitters are disposed uniformly round the magnetic pole M, which is inclined at angle  $\alpha - \beta$  to the rotation axis R. The line of sight cuts the emitters in a circle centred on R. In the two main regions I and III the line of sight cuts the pattern at two different radial distances from the magnetic pole; the existence of the two weak regions II and IV suggests that there may be a radial structure, depicted here as two rings of emitters.

1. The ‘nulls’ in the pulses from PSR B0826–34 are not true ‘nulls’ and the pulsar presents strong and weak emission modes at 1374 MHz. In its strong emission mode, the radiation extends through the whole pulse period, and region I is stronger than region III at this frequency. In the weak emission mode, the profile is similar to that observed in the strong mode at low radio frequency, at which region I is the weaker.

2. Using a phase-tracking method, the drifting subpulses of the pulsar can be traced through the whole pulse period. Thirteen drift bands have been directly observed, covering the whole longitude range, and the drifting occurs in both directions.

3. The subpulses in region I and their spacing ( $P_2$ ) are wider than those in region III. These differences can be accounted for if the magnetic pole is inclined to the rotation axis by about  $0.5^\circ$ .

4. Regions I and III are consistent with radiation from inner and outer cones; in regions II and IV of longitude, the line-of-sight trajectory cuts through a weak emission region between the two cones.

5. The observed direction of drift is a true reversal within the polar cap and is not a product of aliasing with the rotation period.

## REFERENCES

- Biggs J. D., McCulloch P. M., Hamilton P. A., Manchester R. N., Lyne A. G., 1985, MNRAS, 215, 281  
 Davies J. G., Lyne A. G., Smith F. G., Izvekova V. A., Kuzmin A. D., Shitov Y. P., 1984, MNRAS, 211, 57  
 Deich W. T. S., Cordes J. M., Hankins T. H., Rankin J. M., 1986, ApJ, 300, 540

- Durbin J. M., Large M. I., Little A. G., Manchester R. N.,  
Lyne A. G., Taylor J. H., 1979, MNRAS, 186, 39P  
Gil J. A., Lyne A. G., 1995, MNRAS, 276, L55  
Gil J. A., Kijak J., Seiradakis J. H., 1993, A&A, 272, 268  
Gupta Y., Gil J., Kijak J., Sendyk M., 2004, A&A, submitted  
(astro-ph/0404216)  
Hankins T. H., Wolszczan A., 1987, ApJ, 318, 410  
Huguenin G. R., Taylor J. H., Troland T. H., 1970, ApJ, 162, 727  
Kramer M., Wielebinski R., Jessner A., Gil J. A., Seiradakis J. H.,  
1994, A&AS, 107, 515  
Lyne A. G., Ashworth M., 1983, MNRAS, 204, 519  
Lyne A. G., Manchester R. N., 1988, MNRAS, 234, 477  
Manchester R. N., Lyne A. G., Taylor J. H., Durbin J. M.,  
Large M. I., Little A. G., 1978, MNRAS, 185, 409  
Manchester R. N. et al., 2001, MNRAS, 328, 17  
Rankin J. M., 1983, ApJ, 274, 333  
Rankin J. M., 1993a, ApJ, 405, 285  
Rankin J. M., 1993b, ApJS, 85, 145  
Ruderman M. A., Sutherland P. G., 1975, ApJ, 196, 51  
van Leeuwen A. G. J., Kouwenhoven M. L. A., Ramachandran R.,  
Rankin J. M., Stappers B. W., 2002, A&A, 387, 169  
Wright G. A., Fowler L. A., 1981, A&A, 101, 356  
Wright G. A. E., Sieber W., Wolszczan A., 1986, A&A, 160, 402

This paper has been produced using the Royal Astronomical  
Society/Blackwell Science  $\LaTeX$  style file.